Available online at www.sciencedirect.com
ScienceDirect
Journal of Sound and Vibration 322 (2009) 629–651
JOURNAL OF SOUND AND VIBRATION
www.elsevier.com/locate/jsvi

Review

Experimental study of delayed feedback control for a flexible plate

Chen Long-Xiang, Cai Guo-Ping*, Pan Ji

Department of Engineering Mechanics, Shanghai Jiaotong University, Shanghai 200240, PR China

Received 4 May 2008; received in revised form 2 October 2008; accepted 28 November 2008
Handling Editor: J. Lam
Available online 20 January 2009

Abstract

Delayed feedback control is a novel control strategy that utilizes time delay for good control effectiveness. This strategy is now mainly studied on theoretical basis and few effect was ever made on the experiment. This paper presents an experimental study of delayed feedback control using a flexible plate as research object. A treating method for multiple time delays is proposed. The experiment system is structured based on the DSP TMS320F2812. Piezoelectric (PZT) patches are used as actuators and foil gauges as sensors. The optimal positions of PZT actuators on the plate are determined using the particle swarm optimizer (PSO). The feasibility and efficiency of delayed feedback control method are verified both theoretically and experimentally.

Contents

*Corresponding author.
E-mail address: caigp@sjtu.edu.cn (G.-P. Cai).

0022-460X/$ - see front matter © 2008 Elsevier Ltd. All rights reserved.
doi:10.1016/j.jsv.2008.11.045

1. Introduction

Time delay inevitably exists in active control systems and it may cause degradation of control efficiency or even instability of control systems [1]. Many factors, such as measurement of system variables, calculation of controller and processes for actuators to build up required control forces, can result in the non-synchronization of control forces. In practice, many engineering problem exist time delay, such as satellite communication with the ground, control loops of active vehicle suspension system and metal cutting chatter etc. Although in most cases time delay in a control system is small, it leads still to complex dynamic behavior of control systems [1].

Generally speaking, the investigations on time delay may be divided into two classes: elimination and utilization technologies. At first, time delay was regarded as a "bad" factor and had only negative effect on control systems, causing degradation of control efficiency or the instability of systems. In order to eliminate or weaken its negative effect, some methods were subsequently proposed to handle the problem, including Taylor series expansion [2], phase shift technique [3] and advance state estimation [4]. These methods can deal effectively with some small time delay problems in control systems, but awkwardly with large ones. Cai and Huang [5,6] have recently proposed a new time-delay controller. This controller is designed directly from time-delay differential equation without any hypothesis in whole process of controller, suitable for both small and large time delays. The key point of the methods mentioned above to eliminate the negative effect of time delay is so-called time-delay elimination technology or time-delay compensation technology. Its main function is to eliminate or weaken the negative effect of time delay on control efficiency. Moreover, recent investigations have shown that voluntary introduction of delays can also benefit the control. Utilizing time delay to compose a delayed feedback control loop may be used to improve control performance or system stability. For example, in nonlinear dynamics area, achievement is remarkable using time delay to control chaos motion [7–9]. The results obtained in Ref. [9] show that time delay may be used as a simple but efficient "switch" to control motions of a system: either from order motion to chaos or from chaotic motion to order for different applications. In structural control area, Hosek and Olgac [10] developed a time-delay resonator that may be used for vibration control of structures. The main idea of time-delay resonator is to add a delayed feedback loop into control systems to reduce structural vibration by adjusting control weighting coefficient and the magnitude of time delay. Zhao and Xu [11] discussed a delayed feedback control for vibration suppression of a two-degree-of-freedom (dof) nonlinear system with external excitation. Effects of both positive and negative feedback control were observed when the primary resonance and 1:1 internal resonance occur in the system simultaneously. In robotics area, Cai and Lim [12] designed a time-delay controller for a flexible manipulator. Their results show that delayed feedback control design may possibly achieve much better control efficiency than the control design without time delay. Moreover, in control system of pipeline transport, time delay may be utilized to enhance steady critical speed of flowing liquid [13]. Time delay may be also used to improve system stability [14,15]. Those researches above involving the active utilization of time delay is so-called time-delay utilization technology or delayed feedback control method, which assumes time delay as a design parameter to obtain good control performance. Even though up to now researches have been done much on the elimination and utilization of time delay, most of work is theoretical one but few on experiment.

In this paper, the delayed feedback control is numerically and experimentally studied using a flexible plate as a research object. And single and double time delay are considered, respectively. The feasibility and efficiency of the delayed feedback control are verified simultaneously. This paper is organized as follows. Section 2 presents the motion equation of piezoelectric (PZT) flexible cantilever plate. Optimal positions of actuators using the particle swarm optimizer (PSO) are discussed in Section 3. Section 4 gives a discretized state equation of the system with multiple time delays and a corresponding controller. Numerical and experimental results are shown in Section 5 in the consideration of the proposed controller. Finally, concluding remarks are given in Section 6.

2. Equation of motion

Transverse vibration of a flexible cantilever plate is considered, as shown in Fig. 1. Assume that r_1 PZT actuators are used for vibration control of the plate. Based on the Kirchhoff–Love hypothesis, the motion

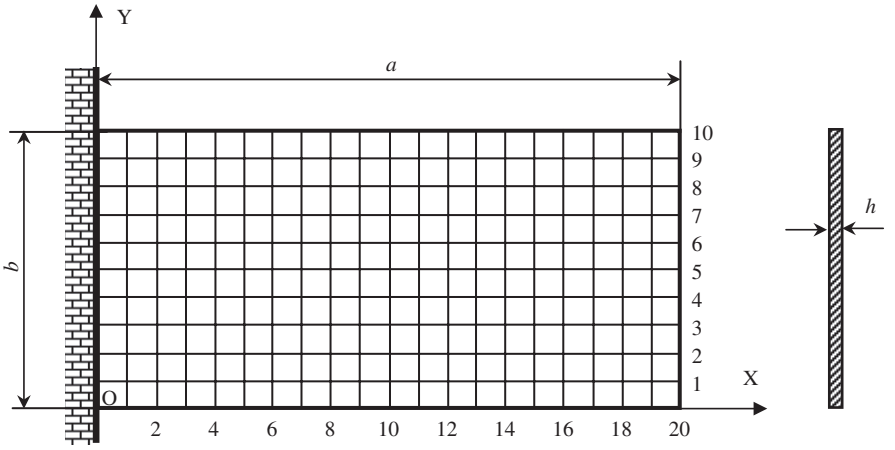

Fig. 1. Cantilever plate with FEM girding.

equation of the plate can be expressed as [16]

$$D_p\nabla^4 w + C_s\dot{w} + \rho_p h\ddot{w} + \sum_{i=1}^{r_1}\left\{ C_0^i \frac{d_{31i}}{h_{ai}}[\delta'(x-x_{1i}) - \delta'(x-x_{2i})][H(y-y_{1i}) - H(y-y_{2i})] + C_0^i \frac{d_{31i}}{h_{ai}}[H(x-x_{1i}) - H(x-x_{2i})][\delta'(y-y_{1i}) - \delta'(y-y_{2i})]\right\} V_i(t) = 0 \quad (1)$$

where $w(x,y,t)$ represents the transverse displacement of any point (x,y) of the plate at the moment t; $D_p = E_p h^3/[12(1-v_p^2)]$ is the flexural rigidity of the plate, E_p and v_p are the Young's modulus and Poisson's ratio of the plate, respectively; $\nabla^2 = \partial^2/\partial x^2 + 2(\partial^2/\partial x\partial y) + \partial^2/\partial y^2$; C_s, the structural damping operator; ρ_p, the mass per unit volume of the plate; h, the thickness of the plate; d_{31i}, the bending strain constant of the i-th PZT actuator; h_{ai}, the thickness of the i-th PZT actuator; $\delta(\cdot)$, the Dirac delta function; (x_{1i}, y_{1i}) and (x_{2i}, y_{2i}) are the down-left and top-right coordinates of the i-th PZT actuator in the O–XY system, respectively; $H(\cdot)$ represents the unit Heaviside (step) function; V_i is the applied voltage on the i-th PZT actuator. The parameter C_0^i in Eq. (1) is the mechanical–electrical coupling coefficient between the i-th PZT actuator and the plate and is given by Ref. [16]

$$C_0^i = -\frac{2}{3}\frac{1+v_{pei}}{1-v_p}\frac{E_p h_p^2 P_i}{1+v_p-(1+v_{pei})P_i} \quad \text{and} \quad P_i = -\frac{E_{pei}}{E_p}\frac{1-v_p^2}{1-v_{pei}^2}\frac{3h_{ai}h_p(2h_p+h_{ai})}{2(h_p^3+h_{ai}^3)+3h_p h_{ai}^2} \quad (2)$$

where E_{pei} and v_{pei} represent the Young's modulus and Poisson's ratio of the i-th PZT actuator, respectively; h_p, the half thickness of the plate.

The transverse displacement $w(x,y,t)$ can be expressed as a time-dependent weighted sum of assumed spatial mode shape functions, given by

$$w(x,y,t) = \sum_{j=1}^{\infty} W_j(x,y)\eta_j(t) \quad (3)$$

where W_j and η_j represent the modal function and modal coordinate of the j-th mode of plate, respectively.

Analytical solution of modal function of the plate cannot be obtained directly, so modal trail function method is often used to express the modal function approximately. In this paper, the modal function is determined in term of the following process: the discrete mode of the plate is firstly obtained using the finite element method (FEM), then the discrete mode is fitted to be a continuous one by polynomial fitting using the classical least squares method. The continuous modal function obtained has also characteristics of orthogonality.

Using the orthogonality of modal function and truncating the first n modes of the plate, the dynamic equation of the plate may be written as

$$\ddot{\hat{\mathbf{\Phi}}}(t) + \hat{\mathbf{C}}\dot{\hat{\mathbf{\Phi}}}(t) + \hat{\mathbf{K}}\hat{\mathbf{\Phi}}(t) = \sum_{i=1}^{r_1} \hat{\mathbf{H}}_i V_i(t) = \hat{\mathbf{H}}\hat{\mathbf{V}}(t) \tag{4}$$

where $\hat{\mathbf{\Phi}}(t) = [\eta_1, \eta_2, \ldots, \eta_n]^{\mathrm{T}}$ is the n-dimensional vector of modal coordinate, T denotes the transpose of a matrix or vector, n is the number of dof of the plate; $\hat{\mathbf{C}} = \mathrm{diag}(2\zeta_1\omega_1, 2\zeta_2\omega_2, \ldots, 2\zeta_n\omega_n)$ is the $n \times n$ damping matrix of the plate, ζ_j and ω_j are the damping ratio and natural frequency of the plate, $j = 1,2,\ldots,n$; $\hat{\mathbf{K}} = \mathrm{diag}(\omega_1^2, \omega_2^2, \ldots, \omega_n^2)$ is the $n \times n$ stiffness matrix of the plate; $\hat{\mathbf{H}}_i = \hat{\mathbf{M}}^{-1}[\mathrm{piezo}_1^i, \mathrm{piezo}_2^i, \ldots, \mathrm{piezo}_n^i]^{\mathrm{T}}$ is a $n \times 1$ vector denoting the positions of actuators, $\hat{\mathbf{M}}$ is the $n \times n$ modal mass matrix of the plate; $\hat{\mathbf{H}} = [\hat{\mathbf{H}}_1, \hat{\mathbf{H}}_2, \ldots, \hat{\mathbf{H}}_{r_1}]$ is a $n \times r_1$ matrix; $\hat{\mathbf{V}}(t) = [V_1(t), V_2(t), \ldots, V_{r_1}(t)]^{\mathrm{T}}$ is a $r_1 \times 1$ vector of PZT voltages. The coefficient of PZT actuator, piezo_j^i, is given by Ref. [16]

$$\begin{aligned} \mathrm{piezo}_j^i = -\Bigg\{ & C_0^i \frac{d_{31i}}{h_{ai}} \left[\int_{y_{1i}}^{y_{2i}} W_{jx}(x_{2i}, y)\,\mathrm{d}y - \int_{y_{1i}}^{y_{2i}} W_{jx}(x_{1i}, y)\,\mathrm{d}y \right] \\ & + C_0^i \frac{d_{31i}}{h_{ai}} \left[\int_{y_{1i}}^{y_{2i}} W_{jy}(x, y_{2i})\,\mathrm{d}y - \int_{y_{1i}}^{y_{2i}} W_{jy}(x, y_{1i})\,\mathrm{d}y \right] \Bigg\} \end{aligned} \tag{5}$$

where $W_{jx} = \partial W_j/\partial x$ and $W_{jy} = \partial W_j/\partial y$.

In the state–space representation, Eq. (4) becomes

$$\dot{\hat{\mathbf{Z}}}(t) = \hat{\mathbf{A}}\hat{\mathbf{Z}}(t) + \hat{\mathbf{B}}\hat{\mathbf{V}}(t) \tag{6}$$

where

$$\hat{\mathbf{Z}}(t) = \begin{bmatrix} \hat{\mathbf{\Phi}}(t) \\ \dot{\hat{\mathbf{\Phi}}}(t) \end{bmatrix}, \quad \hat{\mathbf{A}} = \begin{bmatrix} \mathbf{0} & \mathbf{I} \\ -\hat{\mathbf{K}} & -\hat{\mathbf{C}} \end{bmatrix} \quad \text{and} \quad \hat{\mathbf{B}} = \begin{bmatrix} \mathbf{0} \\ \hat{\mathbf{H}} \end{bmatrix}.$$

3. Optimal positions of actuators

In this section, optimal positions of actuators on the plate will be investigated. To determine positions of actuators is in fact an optimization problem which can be solved by optimizing a certain index function by some optimization algorithm. The index function is to evaluate the optimum of the structure when actuators are placed at different positions on the structure. The extremum of the index function corresponds to the optimal position of the actuator, while the optimization algorithm is to get the extremum as fast as possible. Therefore the optimization problem of actuators consists of the selection of an index function and the selection of an optimization algorithm. For the index function, the index criterion based on controllable Gramian matrix is often used as objective function to optimize the positions of actuators. For example, Sylvaine et al. [17] proposed an index criterion for optimal positions of PZT sensors and actuators of flexible structures using controllable Gramian matrix. This criterion is depended on the geometric characteristics of ellipsoids. The system is more controllable when the value of this criterion is bigger. So the maximum value of this index criterion gives out the best positions of actuators. Wang et al. [18] used this index criterion to study optimal position of one actuator on a two-dimensional (2-D) flexible plate. The index criterion in Ref. [17] is given by

$$\mathrm{Crit} = \mathrm{tr}(\mathbf{W}_c)\sqrt[2n]{\det \mathbf{W}_c}/\sigma(\gamma_i) \tag{7}$$

where $\mathrm{tr}(\mathbf{W}_c)$ is the trace of $\mathbf{W}_c$, representing the total energy transmitted from the actuators to the structure, $\mathbf{W}_c$ is the controllable Gramian matrix that is given by the following Eq. (8); $\sqrt[2n]{\det \mathbf{W}_c}$ is the geometric mean of eigenvalues, namely the volume of the ellipsoids, n is the dof of the structure, $\det W_c$ represents the determinantal value of $\mathbf{W}_c$; $\sigma(\gamma_i)$ is the standard deviation of the eigenvalue of $\mathbf{W}_c$, γ_i is the eigenvalue of $\mathbf{W}_c$.

The parameter $\sigma(\gamma_i)$ penalizes the positions where there are very high or small eigenvalues. The parameter $\mathbf{W}_c$ is the solution of the following Lyapunov equation

$$\hat{\mathbf{A}}\mathbf{W}_c + \mathbf{W}_c\hat{\mathbf{A}}^{\mathrm{T}} + \hat{\mathbf{B}}\hat{\mathbf{B}}^{\mathrm{T}} = \mathbf{0} \tag{8}$$

Next consider the optimization algorithm. In this paper, PSO, proposed by Kennedy and Eberhart in 1995 [19], is used as optimization algorithm for optimal positions of actuators. PSO is one of the evolutionary computation techniques. For its simplicity to use, high-calculation efficiency, fast convergence rate and strong paralleling ability, it has found applications in various scientific problems such as the optimization of continuous nonlinear function, training of artificial neural network weights, fuzzy control, etc. PSO proves effective and efficient in all these applications [19–21].

In a PSO system, each particle represents a candidate solution to the problem at hand. Particles change their positions by flying around in a multidimensional search space until a relatively unchanged position has been encountered, or until computational limitations are exceeded.

Assume that there is a swarm composed of m particles in a D-dimensional space. The position of the i-th particle in the D-dimensional space is represented by a vector $x_i(t) = [x_{i,1}(t), x_{i,2}(t), \ldots, x_{i,D}(t)]^{\mathrm{T}}$ and its motion velocity is $v_i(t) = [v_{i,1}(t), v_{i,2}(t), \ldots, v_{i,D}(t)]^{\mathrm{T}}$, where $x_{i,j}(t)$ and $v_{i,j}(t)$ are the position and velocity of the i-th particle with respect to the j-th dimension in the D-dimensional space, respectively. As a particle moves through the search space, it compares its fitness value at the current position to the best fitness value it has ever attained at any time up to the current time. The best position associated with the best fitness encountered so far is called the individual best $x^*(t)$. For each particle in the swarm, $x^*(t)$ can be determined and updated during the search. In a maximization problem with objective function Crit, the individual best of the i-th particle $x_i^*(t)$ is determined so that $\mathrm{Crit}[x_i^*(t)] \geqslant \mathrm{Crit}[x_i(\tau)]$, $\tau \leqslant t$. For simplicity, assume that $\mathrm{Crit}_i^* = \mathrm{Crit}[x_i^*(t)]$. For the i-th particle, individual best can be expressed as $x_i^*(t) = [x_{i,1}^*(t), x_{i,2}^*(t), \ldots, x_{i,D}^*(t)]^{\mathrm{T}}$. Assume that $x_g^*(t)$ is the best position among all of the individual best positions achieved so far. Hence, the global best can be determined such that $\mathrm{Crit}[x_g^*(t)] \geqslant \mathrm{Crit}[x_i^*(t)]$, $i = 1,2,\ldots,m$. For simplicity, assume that $\mathrm{Crit}_g^* = \mathrm{Crit}[x_g^*(t)]$. In using the PSO, stopping criteria should be defined such that the search process will terminate. In this study, the search will terminate if one of the following criteria is satisfied: (a) the number of iterations since the last change of the best solution is greater than a prespecified number and (b) the number of iterations reaches the maximum allowable number.

The PSO technique can be described in the following steps [20]:

Step 1 (*Initialization*): Set $t = 0$ and generate random m particles, $\{x_i(0), i = 1, 2, \ldots, m\}$, where $x_i(0) = [x_{i,1}(0), x_{i,2}(0), \ldots, x_{i,D}(0)]^{\mathrm{T}}$. $x_{i,d}(0)$ is generated by randomly selecting a value with uniform probability over the d-th optimized parameter search space $[x_d^{\min}, x_d^{\max}]$. Similarly, generate randomly initial velocities of all particles, $\{v_i(0), i = 1, 2, \ldots, m\}$, where $v_i(0) = [v_{i,1}(0), v_{i,2}(0), \ldots, v_{i,D}(0)]^{\mathrm{T}}$. $v_{i,d}(0)$ is generated by randomly selecting a value with uniform probability over the d-th dimension $[-v_d^{\max}, v_d^{\max}]$, where $v_d^{\max}$ is a constant and given by the user. Each particle in the initial population is evaluated using the objective function, Crit. For each particle, set $x_i^*(0) = x_i(0)$ and $\mathrm{Crit}_i^* = \mathrm{Crit}_i$, $i = 1,2,\ldots,m$. Search for the best value of the objective function $\mathrm{Crit}_{\mathrm{best}}$. Set the particle associated with $\mathrm{Crit}_{\mathrm{best}}$ as the global best, $x_g^*(0)$, with an objective function of Crit_g^*. Set the initial value of the inertia weight $\overline{\omega}(0)$ (see Eq. (9)).

Step 2 (*Time updating*): Set $t = t + 1$.

Step 3 (*Weight updating*): Set $\overline{\omega}(t) = \overline{\omega}(t-1)$.

Step 4 (*Velocity updating*): Using the global best and individual best, the i-th particle velocity in the d-th dimension is updated according to the following equation:

$$v_{i,d}(t) = \overline{\omega}(t)v_{i,d}(t-1) + c_1r_1[x_{i,d}^*(t-1) - x_{i,d}(t-1)] + c_2r_2[x_{g(i,d)}^*(t-1) - x_{i,d}(t-1)] \tag{9}$$

where $i = 1, 2, \ldots, m$; $d = 1, 2, \ldots, D$. The parameter $\overline{\omega}(t)$ is the weighting function for velocity of the i-th particle, used to control the impact of the previous velocities on the current velocity. It influences the tradeoff between the global and local exploration abilities of the particles [21]. For initial stages of the search process, large inertia weight to enhance the global exploration is recommended while, for last stages, the inertia weight is reduced for better local exploration. The parameters c_1 and c_2 are positive constants and r_1 and r_2 are uniformly distributed random numbers in [0,1]. Check the velocity limits. If the velocity violated its limit, set it at its proper limit.

Step 5 (*Position updating*): Based on the updated velocities, each particle changes its position according to the following equation:

$$x_{i,d}(t) = x_{i,d}(t-1) + v_{i,d}(t) \tag{10}$$

Step 6 (*Individual best updating*): Each particle is evaluated according to the updated position. If $\mathrm{Crit}_i < \mathrm{Crit}_i^*$, $i = 1,2,\ldots,m$, then update individual best as $x_i^*(t) = x_i(t)$ and $\mathrm{Crit}_i^* = \mathrm{Crit}_i$ and go to step 7; else go to step 7.

Step 7 (*Global best updating*): Search for the maximum value $\mathrm{Crit}_{\max}$ among Crit_i^*, where max is the index of the particle with maximum objective function value, i.e., $\max \in \{i;\ i = 1,2,\ldots,m\}$. If $\mathrm{Crit}_{\max} > \mathrm{Crit}_g^*$ then update global best as $x_g^* = x_{\max}(t)$ and $\mathrm{Crit}_g^* = \mathrm{Crit}_{\max}$ and go to step 8; else go to step 8.

Step 8 (*Stopping criteria*): If one of the stopping criteria is satisfied, then stop, or else go to step 2.

4. Design of multiple time-delay controller

In this section, the controller with multiple time delays is studied. For simplicity in expression, two PZT actuators are used for controlling the first two modes of the plate. The analysis method below may be easily extended to multiple time delays. Setting $n = 2$ and $r_1 = 2$ in Eq. (4) and adding delays in control, the controlled modal equation of the plate may be written as

$$\ddot{\mathbf{\Phi}}(t) + \mathbf{C}\dot{\mathbf{\Phi}}(t) + \mathbf{K}\mathbf{\Phi}(t) = \sum_{i=1}^{2} \mathbf{H}_i V_i(t-\lambda_i) \tag{11}$$

where $\mathbf{\Phi}(t) = [\eta_1, \eta_2]^{\mathrm{T}}$; $\mathbf{C} = \mathrm{diag}(2\zeta_1\omega_1, 2\zeta_2\omega_2)$; $\mathbf{K} = \mathrm{diag}(\omega_1^2, \omega_2^2)$; λ_i represents the time delay, $i = 1,2$; $\mathbf{H}_i = \hat{\mathbf{M}}_{2\times2}^{-1}[\mathrm{piezo}_1^i, \mathrm{piezo}_2^i]^{\mathrm{T}}$, $i = 1,2$, $\hat{\mathbf{M}}_{2\times2}$ is the 2×2 modal mass matrix consisted of the first two modes of the plate, piezo_j^i is given in Eq. (5).

4.1. Discretization and standard of multiple time-delay control equation

The time delay λ_i can be written as

$$\lambda_i = l_i T - \overline{m}_i, \quad i = 1,2 \tag{12}$$

where T is data sampling period, $l_i > 1$ is a positive integral number and $0 \leqslant \overline{m}_i < T$. It is pointed out in Ref. [22] that time delay has small effect on control performance and can be ignored in control design if time delay is smaller than data sampling period T. Time delay affects control system only when it is larger than T. So $\lambda_i > T$ is considered in this paper. Moreover, $\overline{m}_i = 0$ is only considered, i.e., time delay is integer times of sampling period.

In the state–space representation, Eq. (11) becomes

$$\dot{\mathbf{Z}}(t) = \mathbf{A}\mathbf{Z}(t) + \sum_{i=1}^{2} \mathbf{B}_i V_i(t-\lambda_i) \tag{13}$$

where

$$\mathbf{Z}(t) = \begin{bmatrix} \mathbf{\Phi}(t) \\ \dot{\mathbf{\Phi}}(t) \end{bmatrix}, \quad \mathbf{A} = \begin{bmatrix} \mathbf{0} & \mathbf{I} \\ -\mathbf{K} & -\mathbf{C} \end{bmatrix} \quad \text{and} \quad \mathbf{B}_i = \begin{bmatrix} \mathbf{0} \\ \mathbf{H}_i \end{bmatrix}.$$

The analytical solution of Eq. (13) is [5,22]

$$\mathbf{Z}(t) = \mathrm{e}^{\mathbf{A}(t-t_0)}\mathbf{Z}(t_0) + \sum_{i=1}^{2} \int_{t_0}^{t} \mathrm{e}^{\mathbf{A}(t-\tau)}\mathbf{B}_i V_i(\tau-\lambda_i)\,\mathrm{d}\tau \tag{14}$$

Zero-order holder is used in the structure, i.e.,

$$V_i(t) = V_i(k), \quad kT \leqslant t < (k+1)T \tag{15}$$

Let $t_0 = kT$ and $t = (k+1)T$, Eq. (14) becomes

$$\mathbf{Z}(k+1) = \mathbf{e}^{\mathbf{A}T}\mathbf{Z}(k) + \sum_{i=1}^{2} \int_{kT}^{(k+1)T} \mathrm{e}^{\mathbf{A}((k+1)T-\tau)}\mathbf{B}_i V_i(\tau - \lambda_i)\,\mathrm{d}\tau \tag{16}$$

By variable substitution $\eta = (k+1)T - \tau$, Eq. (16) becomes

$$\mathbf{Z}(k+1) = \mathrm{e}^{\mathbf{A}T}\mathbf{Z}(k) + \sum_{i=1}^{2} \int_{0}^{T} \mathrm{e}^{\mathbf{A}\eta}\mathbf{B}_i V_i[(k+1)T - l_i T + \overline{m}_i - \eta]\,\mathrm{d}\eta \tag{17}$$

With $\overline{m}_i = 0$ and substitution of Eq. (15) into Eq. (17), we have

$$\mathbf{Z}(k+1) = \mathbf{F}\mathbf{Z}(k) + \sum_{i=1}^{2} \mathbf{G}_i V_i(k - l_i) \tag{18}$$

where $\mathbf{F} = \mathrm{e}^{\mathbf{A}T}$ and $\mathbf{G}_i = \int_0^T \mathrm{e}^{\mathbf{A}\tau}\,\mathrm{d}\tau\,\mathbf{B}_i$, $i = 1,2$.

Eq. (18) is a time-delay differential equation. Next consider the standardization of this equation. Augmenting the state variables in Eq. (18) as

$$\begin{cases} Z_{4+1}(k) = V_1(k - l_1) \\ \vdots \\ Z_{4+l_1}(k) = V_1(k-1) \\ Z_{4+l_1+1}(k) = V_2(k - l_2) \\ \vdots \\ Z_{4+l_1+l_2}(k) = V_2(k-1) \end{cases} \tag{19}$$

and defining a new state vector as

$$\overline{\mathbf{Z}}(k) = [\mathbf{Z}(k), Z_{4+1}(k), \ldots, Z_{4+l_1+l_2}(k)]^{\mathrm{T}} \tag{20}$$

Thus, Eq. (18) can be changed into the following standard discrete form without any explicit time delay

$$\overline{\mathbf{Z}}(k+1) = \overline{\mathbf{F}}\,\overline{\mathbf{Z}}(k) + \overline{\mathbf{G}}\mathbf{V}(k) \tag{21}$$

where

$$\mathbf{V}(k) = \begin{bmatrix} V_1(k) \\ V_2(k) \end{bmatrix}, \quad \overline{\mathbf{F}} = \begin{bmatrix} \mathbf{F} & \mathbf{G}_1 & \mathbf{0} & \cdots & \mathbf{0} & \mathbf{G}_2 & \mathbf{0} & \cdots & \mathbf{0} \\ \mathbf{0} & 0 & 1 & \cdots & 0 & 0 & 0 & \cdots & 0 \\ \vdots & \vdots & \vdots & \ddots & \vdots & \vdots & \vdots & \cdots & \vdots \\ \mathbf{0} & 0 & 0 & \cdots & 1 & 0 & 0 & \cdots & 0 \\ \mathbf{0} & 0 & 0 & \cdots & 0 & 0 & 0 & \cdots & 0 \\ \mathbf{0} & 0 & 0 & \cdots & 0 & 0 & 1 & \cdots & 0 \\ \vdots & \vdots & \vdots & \cdots & \vdots & \vdots & \vdots & \ddots & \vdots \\ \mathbf{0} & 0 & 0 & \cdots & 0 & 0 & 0 & \cdots & 1 \\ \mathbf{0} & 0 & 0 & \cdots & 0 & 0 & 0 & \cdots & 0 \end{bmatrix} \quad \text{and} \quad \overline{\mathbf{G}} = \begin{bmatrix} \mathbf{0} & \mathbf{0} \\ 0 & 0 \\ \vdots & \vdots \\ 0 & 0 \\ 1 & 0 \\ 0 & 0 \\ \vdots & \vdots \\ 0 & 0 \\ 0 & 1 \end{bmatrix} \tag{22}$$

When $\overline{m}_i \neq 0$ in Eqs. (12) and (13) can be also changed into standard discrete form, for details see Refs. [5,22].

4.2. Controller design

Below controller design is presented using the discrete optimal control method. To achieve good efficiency, the following continuous performance index is used

$$J = \int_0^\infty [\mathbf{Z}^{\mathrm{T}}(t)\overline{\mathbf{Q}}_1\mathbf{Z}(t) + \mathbf{V}^{\mathrm{T}}(t)\overline{\mathbf{Q}}_2\mathbf{V}(t)]\,\mathrm{d}t \tag{23}$$

where $\overline{\mathbf{Q}}_1$ is non-negative definite symmetric matrix and $\overline{\mathbf{Q}}_2$ is positive definite symmetric matrix. The performance index, Eq. (23), is a continuous form so as to guarantee good response efficiency of systems not only on every sampling point but also between any two adjacent sampling points. However, the discrete performance index can only guarantee good efficiency on every sampling point. Surge behavior may possibly exist between sampling points. So the continuous performance index is used as the objective function in this paper. Now the task of control design is to design controller for the system Eq. (13) such that the performance index in Eq. (23) attains minimum. In the above, Eq. (13) has been discretized and changed into the standard discrete form without any explicit time delay. Below the performance index, Eq. (23), will be discretized and changed to be the function of the augmented state. Eq. (23) may be written as the following discrete form

$$J = \sum_{k=0}^{\infty} J_k, \quad J_k = \int_{kT}^{(k+1)T} [\mathbf{Z}^{\mathrm{T}}(t)\overline{\mathbf{Q}}_1\mathbf{Z}(t) + \mathbf{V}^{\mathrm{T}}(t)\overline{\mathbf{Q}}_2\mathbf{V}(t)]\,\mathrm{d}t \tag{24}$$

When $kT \leqslant t < (k+1)T$, the solution of Eq. (13) is

$$\mathbf{Z}(t) = \mathrm{e}^{\mathbf{A}(t-kT)}\mathbf{Z}(k) + \sum_{i=1}^{2} \int_{kT}^{t} \mathrm{e}^{\mathbf{A}(t-\tau)}\,\mathrm{d}\tau\,\mathbf{B}_i V_i(k-l_i) \tag{25}$$

Substituting Eq. (25) into Eq. (24) and then arranging the expression, we have

$$J = \sum_{k=0}^{\infty} \left[\mathbf{Z}^{\mathrm{T}}(k)\mathbf{Q}_1\mathbf{Z}(k) + 2\sum_{i=1}^{2} \mathbf{Z}^{\mathrm{T}}(k)\mathbf{Q}_{0i}V_i(k-l_i) + \sum_{i=1}^{2}\sum_{j=1}^{2} V_i(k-l_i)Q_{ij}V_j(k-l_j) + \mathbf{V}^{\mathrm{T}}(k)\mathbf{Q}_2\mathbf{V}(k) \right] \tag{26}$$

where

$$\begin{cases} \mathbf{Q}_1 = \int_0^T \mathbf{F}^{\mathrm{T}}(t)\overline{\mathbf{Q}}_1\mathbf{F}(t)\mathrm{d}t, \quad \mathbf{Q}_2 = \overline{\mathbf{Q}}_2 T \\ \mathbf{Q}_{0i} = \left[\int_0^T \mathbf{F}^{\mathrm{T}}(t)\overline{\mathbf{Q}}_1\mathbf{G}_{11}(t)\mathrm{d}t\right]\mathbf{B}_i, \quad i = 1,2 \\ Q_{ij} = \mathbf{B}_i^{\mathrm{T}}\left[\int_0^T \mathbf{G}_{11}^{\mathrm{T}}(t)\overline{\mathbf{Q}}_1\mathbf{G}_{11}(t)\,\mathrm{d}t\right]\mathbf{B}_j, \quad i,j = 1,2 \end{cases} \tag{27}$$

where $\mathbf{F}(t) = \mathrm{e}^{\mathbf{A}t}$ and $\mathbf{G}_{11}(t) = \int_0^t \mathrm{e}^{\mathbf{A}\tau}\,\mathrm{d}\tau$.

The performance index Eq. (26) may be rearranged as the following standard form

$$J = \sum_{k=0}^{\infty} [\overline{\mathbf{Z}}^{\mathrm{T}}(k)\hat{\mathbf{Q}}_1\overline{\mathbf{Z}}(k) + \mathbf{V}^{\mathrm{T}}(k)\hat{\mathbf{Q}}_2\mathbf{V}(k)] \tag{28}$$

where

$$\hat{\mathbf{Q}}_1 = \begin{bmatrix} \mathbf{Q}_1 & \mathbf{Q}_{01} & \mathbf{0} & \mathbf{Q}_{02} & \mathbf{0} \\ \mathbf{Q}_{01}^T & Q_{11} & \mathbf{0} & Q_{12} & \mathbf{0} \\ \mathbf{0} & \mathbf{0} & \mathbf{0} & \mathbf{0} & \mathbf{0} \\ \mathbf{Q}_{01}^T & Q_{21} & \mathbf{0} & Q_{22} & \mathbf{0} \\ \mathbf{0} & \mathbf{0} & \mathbf{0} & \mathbf{0} & \mathbf{0} \end{bmatrix} \quad \text{and} \quad \hat{\mathbf{Q}}_2 = \overline{\mathbf{Q}}_2 T \tag{29}$$

Eq. (28) is a standard form of performance index. So the next task is to design optimal controller for the system Eq. (21) by minimizing the objective function given by Eq. (28). This controller may be designed using

the discrete optimal control method, given by Refs. [5,22]

$$\begin{aligned}\mathbf{V}(k) &= -\mathbf{L}\overline{\mathbf{Z}}(k)\\ &= -\mathbf{L}_1\mathbf{Z}(k)-\mathbf{L}_2V_1(k-l_1)-\cdots-\mathbf{L}_{l_1+1}V_1(k-1)-\mathbf{L}_{l_1+2}V_2(k-l_2)-\cdots-\mathbf{L}_{l_1+l_2+1}V_2(k-1)\end{aligned} \quad (30)$$

where $\mathbf{L}_1,\mathbf{L}_2,\ldots,\mathbf{L}_{l_1+l_2+1}$ are the component matrices of $\mathbf{L}$. Parameter $\mathbf{L}$ is given by

$$\mathbf{L}=[\hat{\mathbf{Q}}_2+\overline{\mathbf{G}}^{\mathrm{T}}\mathbf{S}\overline{\mathbf{G}}]^{-1}\overline{\mathbf{G}}^{\mathrm{T}}\mathbf{S}\overline{\mathbf{F}} \quad (31)$$

where $\mathbf{S}$ is the solution of the following discrete Riccati algebraic equation

$$\mathbf{S}=\overline{\mathbf{F}}^{\mathrm{T}}[\mathbf{S}-\mathbf{S}\overline{\mathbf{G}}[\hat{\mathbf{Q}}_2+\overline{\mathbf{G}}^{\mathrm{T}}\mathbf{S}\overline{\mathbf{G}}]^{-1}\overline{\mathbf{G}}^{\mathrm{T}}\mathbf{S}]\overline{\mathbf{F}}+\hat{\mathbf{Q}}_1 \quad (32)$$

We can observe from Eq. (30) that the controller $\mathbf{V}(k)$ at the moment kT contains not only the state term $\mathbf{Z}(k)$ at this moment, but also some control terms before this moment.

Computations for $\mathbf{F}(t)$, $\mathbf{G}_{11}(t)$, $\mathbf{G}_i$, $\mathbf{Q}_1$, $\mathbf{Q}_{0i}$ and Q_{ij} may be found in Refs. [5,22]. They are summed up as follows:

$$\begin{cases}\mathbf{G}_{11}=\mathbf{I}T+\mathbf{O}\mathbf{A}, \quad \mathbf{D}_0=\overline{\mathbf{Q}}_1\mathbf{O}+\mathbf{A}^{\mathrm{T}}\mathbf{W}\\ \mathbf{F}=\mathbf{I}+\mathbf{G}_{11}\mathbf{A}, \quad \mathbf{G}_i=\mathbf{G}_{11}\mathbf{B}_i\\ \mathbf{Q}_1=\overline{\mathbf{Q}}_1\mathbf{G}_{11}+\mathbf{A}^{\mathrm{T}}\mathbf{D}_0^{\mathrm{T}}, \quad \mathbf{Q}_{0i}=\mathbf{D}_0\mathbf{B}_i\\ Q_{ij}=\mathbf{B}_i^{\mathrm{T}}\mathbf{W}\mathbf{B}_j, \quad i,j=1,\ldots,N_a\end{cases} \quad (33)$$

where $\mathbf{O}$ and $\mathbf{W}$ are given by

$$\begin{cases}\mathbf{O}=\sum\limits_{\mathbf{k}=2}^{\infty}\mathbf{O}_k\\ \mathbf{O}_k=\dfrac{\mathbf{A}T}{k}\mathbf{O}_{k-1},\\ \mathbf{O}_2=\dfrac{T^2}{2}\mathbf{I}\end{cases} \quad \begin{cases}\mathbf{W}=\sum\limits_{k=2}^{\infty}\mathbf{W}_k\\ \mathbf{W}_k=\dfrac{T}{k+1}[\mathbf{A}^{\mathrm{T}}\mathbf{W}_{k-1}+\mathbf{W}_{k-1}\mathbf{A}+\overline{\mathbf{Q}}_1\mathbf{V}_k+\mathbf{V}_k^{\mathrm{T}}\overline{\mathbf{Q}}_1]\\ \mathbf{W}_2=\dfrac{\overline{\mathbf{Q}}_1T^3}{3}\end{cases} \quad (34)$$

The parameters $\mathbf{O}$ and $\mathbf{W}$ in Eq. (34) will both converge to constant matrices in limited steps of iterative computation [5,22].

5. Numerical simulations and experimental studies

To demonstrate the feasibility and effectiveness of the proposed time-delay controller, numerical simulations and experiments are carried out in this section. Aluminum alloy plate is adopted as structural model. The length, width and thickness of the plate are $a=600\,\mathrm{mm}$, $b=300\,\mathrm{mm}$ and $h=1.50\,\mathrm{mm}$, respectively, as shown in Fig. 1. Material properties of the plate are as follows: Young's elastic modulus is $E_p=69\,\mathrm{GPa}$, Poisson's ratio is $v_p=0.3$ and density is $\rho_p=2.7\times10^3\,\mathrm{kg/m^3}$. The first two natural frequencies of the plate determined by theoretical model are 3.490 and 15.026 Hz, where the first one corresponds to the bending mode and the second one the torsional mode. The first two natural frequencies determined by experiments are 3.37 and 14.326 Hz. The error between theoretical and experimental results of frequencies is within 5%. The first two damping ratio of the plate are experimentally determined to be 0.0055 and 0.003, respectively.

In the experiments, two PZT patches are used as actuators for controlling the plate. The two PZT actuators have the same size, given by 60 mm × 15 mm × 0.5 mm. Because of the limitation of the length of PZT actuators, they are stuck near the optimal positions determined by the PSO (see Table 1). The middle point of the first PZT patch (denoted by Actuator I) along its length direction is at (0.067 m, 0.0285 m), as shown in Fig. 2 and the delayed time of Actuator I is represented by λ_1. The second PZT patch (denoted by Actuator II) is at (0.45 m, 0.2135 m) and its delayed time is λ_2. The material parameters of PZT actuators are as follows: Young's elastic modulus is $E_{pe}=63\,\mathrm{GPa}$, Poisson's ratio is $v_{pe}=0.35$, PZT strain constants are $d_{31}=1.75\times10^{-10}\,\mathrm{m/V}$ and $d_{36}=0$.

In the experiment, foil gauge is adopted as sensor for measuring strain value of the plate. Strain value can be transformed into transverse displacement in term of the following Eq. (36). Since the maximum strain value of

Table 1
Number and optimal positions of PZT actuators.

Number	1	2	3	4	5	6	7	8	9
Location	(1,1)	(1,1) (15,7)	(1,1) (15,6) (1,9)	(1,1) (15,4) (1,8) (1,9)	(1,1) (1,2) (11,5) (1,8) (1,9)	(1,1) (1,2) (1,3) (17,4) (1,7) (1,9)	(1,1) (1,2) (15,5) (18,8) (1,8) (1,9) (2,8)	(1,1) (1,3) (1,4) (1,6) (1,7) (1,9) (11,5) (12,8)	(1,1) (1,2) (1,6) (1,8) (1,9) (6,5) (11,3) (14,1) (14,6)

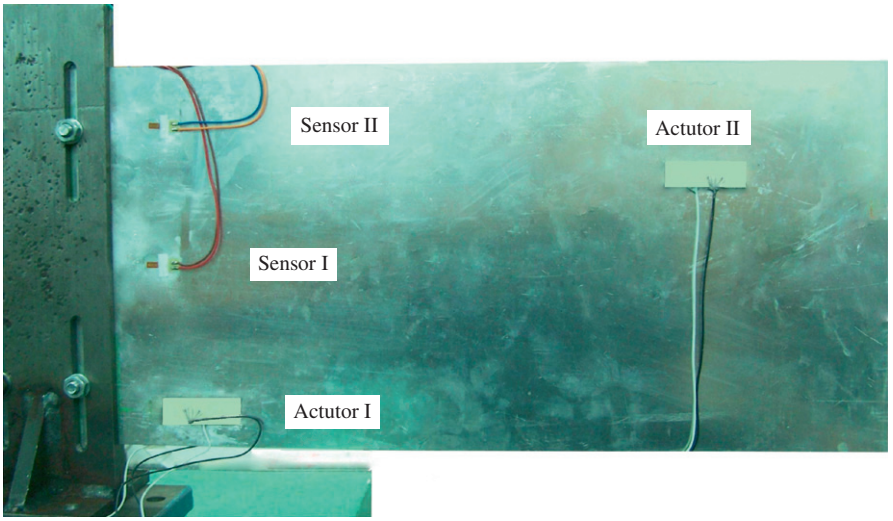

Fig. 2. Photo of experiment plate.

the first modal vibration of the plate lies at the middle point of the fixed end of the plate in Y direction and that of the second modal vibration at the upper position of the fixed end, so two foil gauges, denoted by Sensors I and II, are stuck near these two positions, as shown in Fig. 2. Their coordinates on the plate are (0.031 m, 0.1475 m) and (0.034 m, 0.254 m).

The relationship between bending strain and displacement curvature of the plate is given by

$$\varepsilon_x = \frac{h}{2}\frac{\partial^2 w(x,y,t)}{\partial x^2} \tag{35}$$

where ε_x is the bending strain of the plate in X direction; h, the thickness of the plate; $w(x,y,t)$ and $\partial^2 w(x,y,t)/\partial x^2$ are the transverse displacement and displacement curvature of the plate, respectively. Using $w(x,y,t) = \sum_{i=1}^{r} W_i(x,y)\eta_i(t)$, where r is the number of sensors given in the need of the following experimental studies, Eq. (35) may be changed as

$$w(x,y,t) = \frac{2}{h}[W_1(x,y) \quad \dots \quad W_r(x,y)] \begin{bmatrix} \frac{\partial^2 W_1(x_1,y_1)}{\partial x^2} & \dots & \frac{\partial^2 W_r(x_1,y_1)}{\partial x^2} \\ \vdots & \dots & \vdots \\ \frac{\partial^2 W_1(x_r,y_r)}{\partial x^2} & \dots & \frac{\partial^2 W_r(x_r,y_r)}{\partial x^2} \end{bmatrix}^{-1} \begin{bmatrix} \varepsilon_{x_1} \\ \vdots \\ \varepsilon_{x_r} \end{bmatrix} \tag{36}$$

where (x_i, y_i) is the coordinate of the i-th sensor on the plate, $i = 1,\dots,r$.

5.1. Results of optimal positions of actuators

Assume that one to nine actuators are used for the plate, respectively. And then consider their optimal positions on the plate. According to the method given in Section 3, the FEM is firstly used for the plate so as to obtain the generalized mass and stiffness matrices of the plate, thus the first nine natural frequencies and discrete modes may be obtained. Then the discrete modes may be fitted to be continuous modes using the classical least squares method. Finally the optimal positions of actuators may be calculated using the PSO. In using the PSO, the number of particles is set to be 100, i.e., $m = 100$. The study factors in Eq. (9), c_1 and c_2, are both chosen to be 2, i.e., $c_1 = c_2 = 2$. The parameter $v_{\max}$ is $v_{\max} = 5$. The parameter $\overline{\omega}$ is degressive from 0.9 to 0.5 according to the number of iterative step. The obtained optimal positions of actuators are given in Table 1, where the coordinate draft is shown in Fig. 1.

5.2. Signal difference

In active controller, both displacement and velocity (namely the state of system) are required to be used in control feedback. However, velocity signal (also called differential signal) cannot be measured directly from sensors in practice. It should be estimated from physical sensor measurements and then is used to calculate the control forces. In the initial experiment, it was found that the collected signal by the foil gauge may appear high-frequency noise due to the disturbance of mechanism and electricity, resulting in that differential signal obtained using the classical interpolation method is disorganized. Here we adopt the tracking-differentiator given in Ref. [23] to estimate the differential signal. This differentiator can quickly track input signal and give out high-quality differential signal.

The tracking-differentiator in discrete form is given by Ref. [23]

$$\begin{cases} \overline{x}_1(k+1) = \overline{x}_1(k) + T\overline{x}_2(k) \\ \overline{x}_2(k+1) = \overline{x}_2(k) + T\,\mathrm{fst}(\overline{x}_1(k), \overline{x}_2(k), u(k), \overline{r}, \overline{h}) \end{cases} \tag{37}$$

where $u(k)$ is the input signal at the moment k, $\overline{x}_1$, the tracking signal of $u(k)$, $\overline{x}_2$, the estimated differential signal of $\overline{x}_1$, T, the sampling period, $\overline{r}$, the parameter determining the tracking speed and $\overline{h}$, the parameter determining the filter effect when the input signal is polluted by noise. The fst is given by

$$\mathrm{fst} = \begin{cases} -\overline{r}\,\overline{a}/\delta, & |\overline{a}| \leqslant \delta \\ -\overline{r}\,\mathrm{sgn}(\overline{a}), & |\overline{a}| > \delta \end{cases} \tag{38}$$

where

$$\overline{a} = \begin{cases} \overline{x}_2 + \overline{y}/\overline{h}, & |\overline{y}| \leqslant \delta_0 \\ \overline{x}_2 + 0.5(a_0 - \delta)\mathrm{sgn}(y), & |\overline{y}| > \delta_0 \end{cases}$$

$$\delta = \overline{r}\overline{h}, \quad \delta_0 = \delta\overline{h}, \quad \overline{y} = \overline{x}_1 - u + \overline{h}\overline{x}_2 \quad \text{and} \quad a_0 = \sqrt{\delta^2 + 8\overline{r}|\overline{y}|}$$

$$\mathrm{sgn}(\overline{a}) = \begin{cases} 1, & \overline{a} > 0 \\ 0, & \overline{a} = 0 \\ -1, & \overline{a} < 0 \end{cases}$$

In the experiments, the data sampling period of sensor is chosen as $T = 0.001$ and 0.005 s in the need of the following studies; $\overline{r}$ and $\overline{h}$ are chosen as $\overline{r} = 1000$ and $\overline{h} = 0.005$.

5.3. Experiment system

The experiment system is structured based on the DSP TMS320F2812. This DSP is one of the advanced digital processors nowadays. The DSP deals with the on-line computation of controller in terms of the

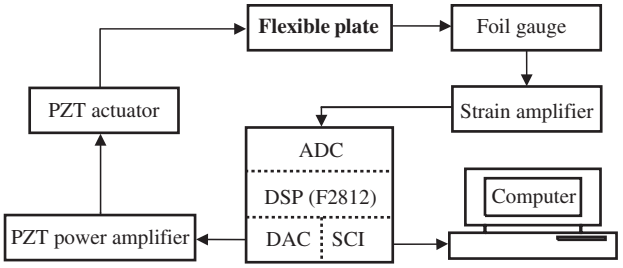

Fig. 3. Flow chart of experiment system.

feedback signal from the foil gauge to get the PZT voltage. The flow chart of experiment system is shown in Fig. 3 and the detailed signal flow and process are as follows:

(1) Feedback signal loop: the signal collected on the foil gauge is amplified by the strain amplifier and then enters the ADC module in DSP.
(2) Control signal loop: the voltage signal goes through the two channels of DAC module into the PZT power amplifier where it gets amplified and then it goes into the two PZT actuators.
(3) The DSP communicates with the peripheral computer via the SCI module which transfers experimental data to the computer to save and to render diagrams.

5.4. Results of single time-delay case

Single time-delay case is firstly considered. Only one PZT actuator, Actuator I, is used for the plate and this actuator is assumed to have time delay. Assume that the initial condition of the plate is $w(0.6,0,0)=0.02\,\mathrm{m}$, $\dot{w}(0.6,0,0)=0$, i.e., the down-right point of the plate has an initial displacement. Under this initial condition, the plate will behave with a free vibration. Since the free vibration of the plate is mainly dominated by its first mode, Actuator I is used for controlling this mode. In addition, Sensor I is used as signal measurement of the plate.

For this case, Eq. (36) becomes

$$w(x,y,t)=2\varepsilon_{x_1}W_1(x,y)\Big/\left(\frac{\partial^2 W_1(x_1,y_1)}{\partial x^2}\times h\right) \tag{39}$$

In the experiments and numerical simulations, the weighting matrices in Eq. (23) are chosen as $\overline{\mathbf{Q}}_1=[100,1]$ and $\overline{\mathbf{Q}}_2=8\times10^{-4}$. The following five cases are considered:

(1a) no time delay in the system; the no-delay controller is used to control the non-time-delay system;
(2a) the time delay $\lambda_1=0.08\,\mathrm{s}$ exists in the system for experiment study and the time delay $\lambda_1=0.08\,\mathrm{s}$ for numerical study; the no-delay controller is used to control the time-delay system;
(3a) $\lambda_1=0.005\,\mathrm{s}$ exists in the system for both experimental and numerical studies; the time-delay controller presented in this paper is used to control the time-delay system;
(4a) $\lambda_1=0.05\,\mathrm{s}$ exists in the system for both experimental and numerical studies; the time-delay controller is used to control the time-delay system and
(5a) $\lambda_1=0.4\,\mathrm{s}$ exists in the system for both experimental and numerical studies; the time-delay controller is used to control the time-delay system.

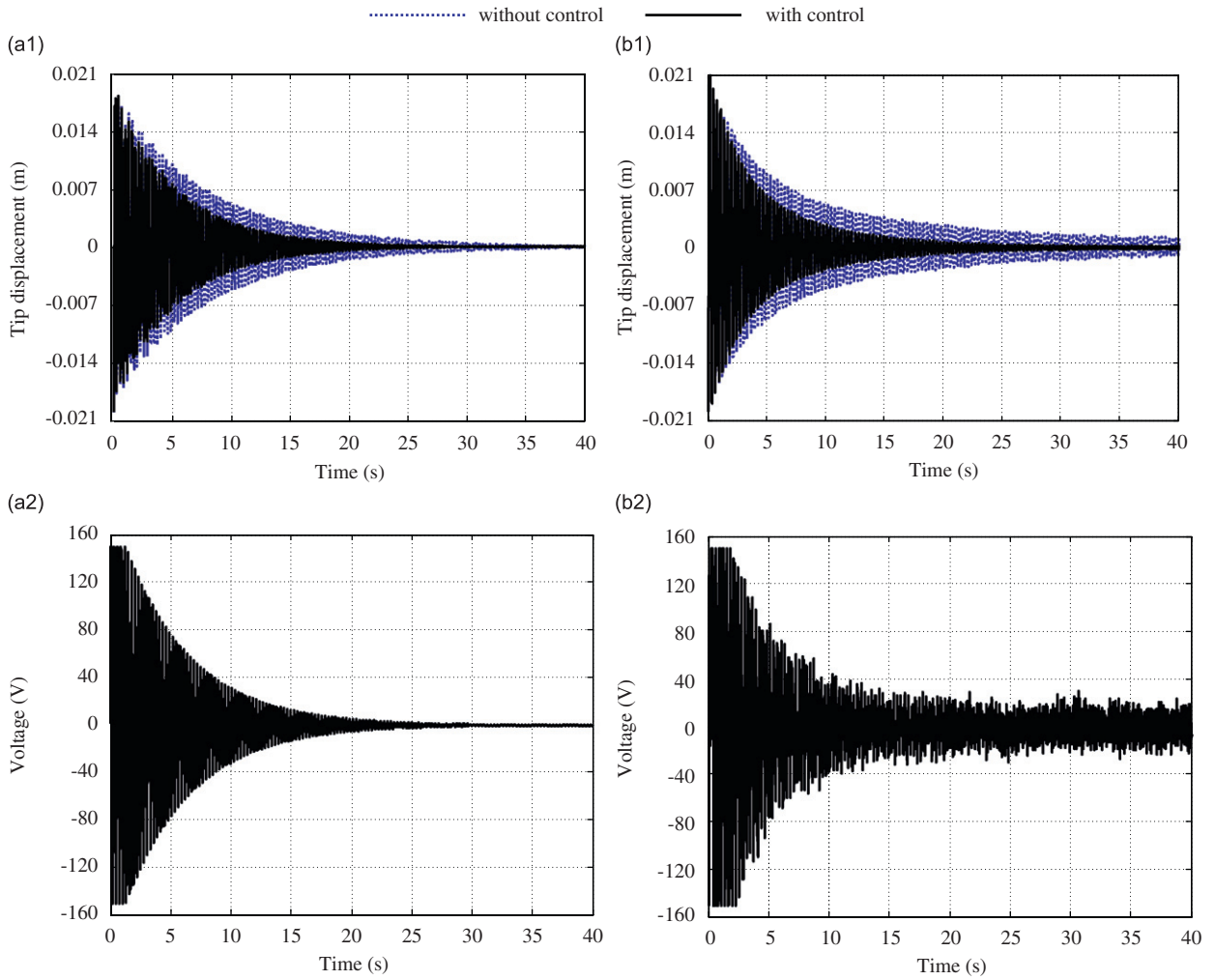

Fig. 4. Response of the plate and applied voltage of Actuator I using the no-delay controller to control the plate without time delay (one actuator case): (a) simulation result and (b) experimental result.

In the experiments for the cases (1a)–(4a), data sampling period of sensor is $T = 0.001$ s. $T = 0.005$ s is taken for the case (5a) in consideration of store capacity of DSP.

Figs. 4–8 show the simulation and experimental results of the responses of the down-right point of the plate and the applied PZT voltage for the above five cases, where Fig. 4 is the result using the no-delay controller to control the non-time-delay system, Fig. 5 using the no-delay controller to control the time-delay system and Figs. 6–8 using the time-delay controller to control the time-delay system. The result without control for the plate is shown in Figs. 4–8 for comparison too. From Fig. 5 we can observe that vibration of the plate cannot be suppressed if time delay is not treated in control design. The response of the plate with control is contrary larger than that without control. The results in Figs. 6–8 show that the proposed time-delay controller is effective in suppressing the vibration of the plate.

It should be mentioned herein that Fig. 5 is the results of disabled delay. The disabled delay of numerical simulation is different from that of experiment study. The disabled delay of experiment study is 0.04 s and that of numerical simulation 0.08 s. This difference is probably caused by some uncertain factors between theoretical and experimental studies, such as model error, parameter uncertainty and signal noise etc. In

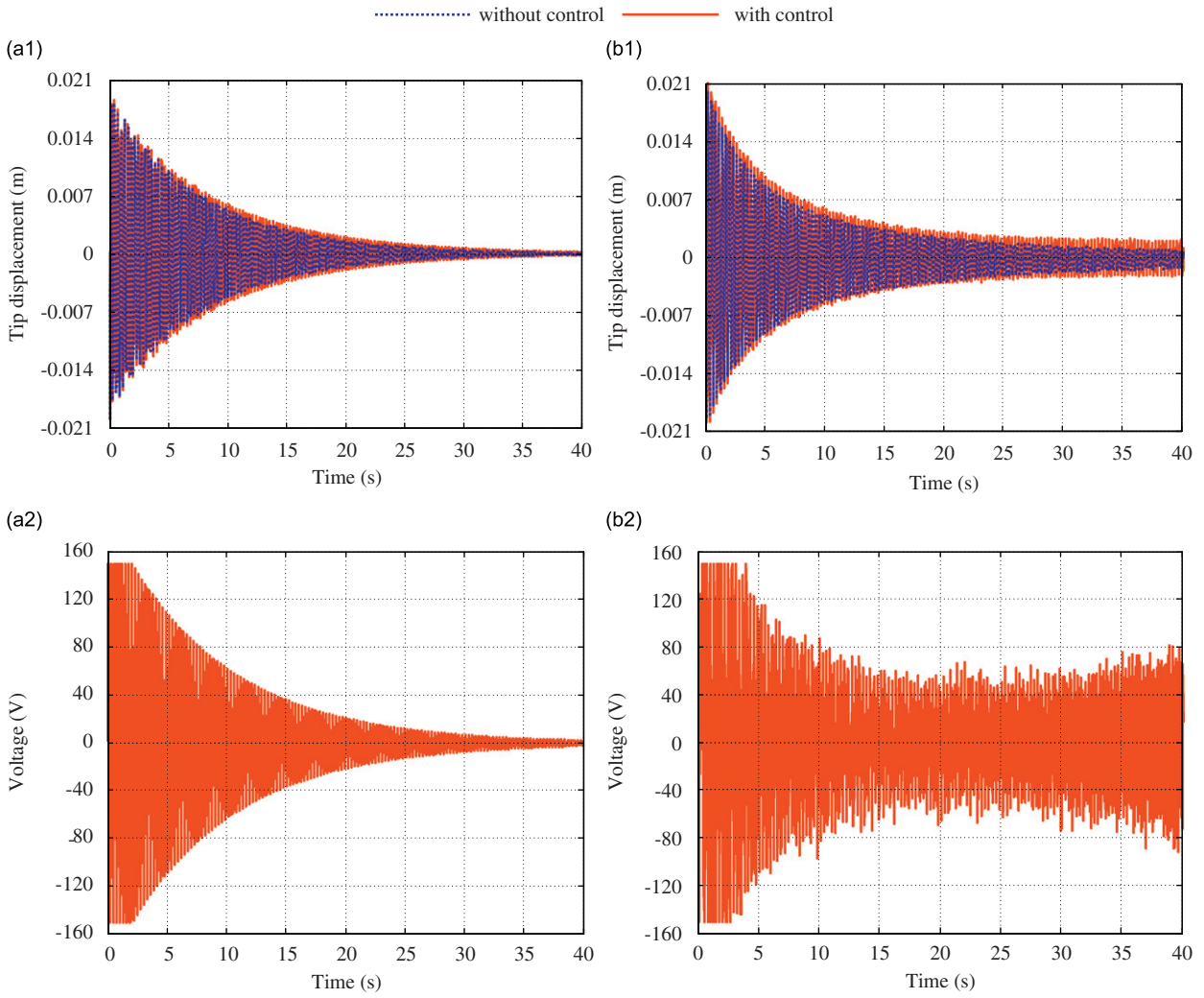

Fig. 5. Response of the plate and applied voltage of Actuator I using the no-delay controller to control the plate with time delay (one actuator case): (a) simulation result ($\lambda_1 = 0.08$ s) and (b) experimental result ($\lambda_1 = 0.04$ s).

addition, the disabled delay of experiment study is smaller than that of numerical simulation. This is reasonable since the simulation result is obtained under ideal condition and many actual factors in the experiment cannot be fully considered in the simulation. The results in Fig. 5 indicate that time delay in control systems may cause deterioration of control efficiency if it is not treated in control design.

5.5. *Results of two time-delay case*

For large or complex flexible structures, more than one actuator is often used for vibration control of structures. Each actuator possibly exist different delay due to the differences of physical parameter and capability of actuators. In this section, multiple time delays are considered. The two PZT actuators, Actuators I and II, are used to control the first two modes of the plate. The delayed time in Actuator I is represented by λ_1 and Actuator II by λ_2. Sensors I and II are both used as signal measurement. As the same in Section 5.4, the down-right point of the plate has an initial condition, $w(0.6, 0, 0) = 0.02$ m and $\dot{w}(0.6, 0, 0) = 0$.

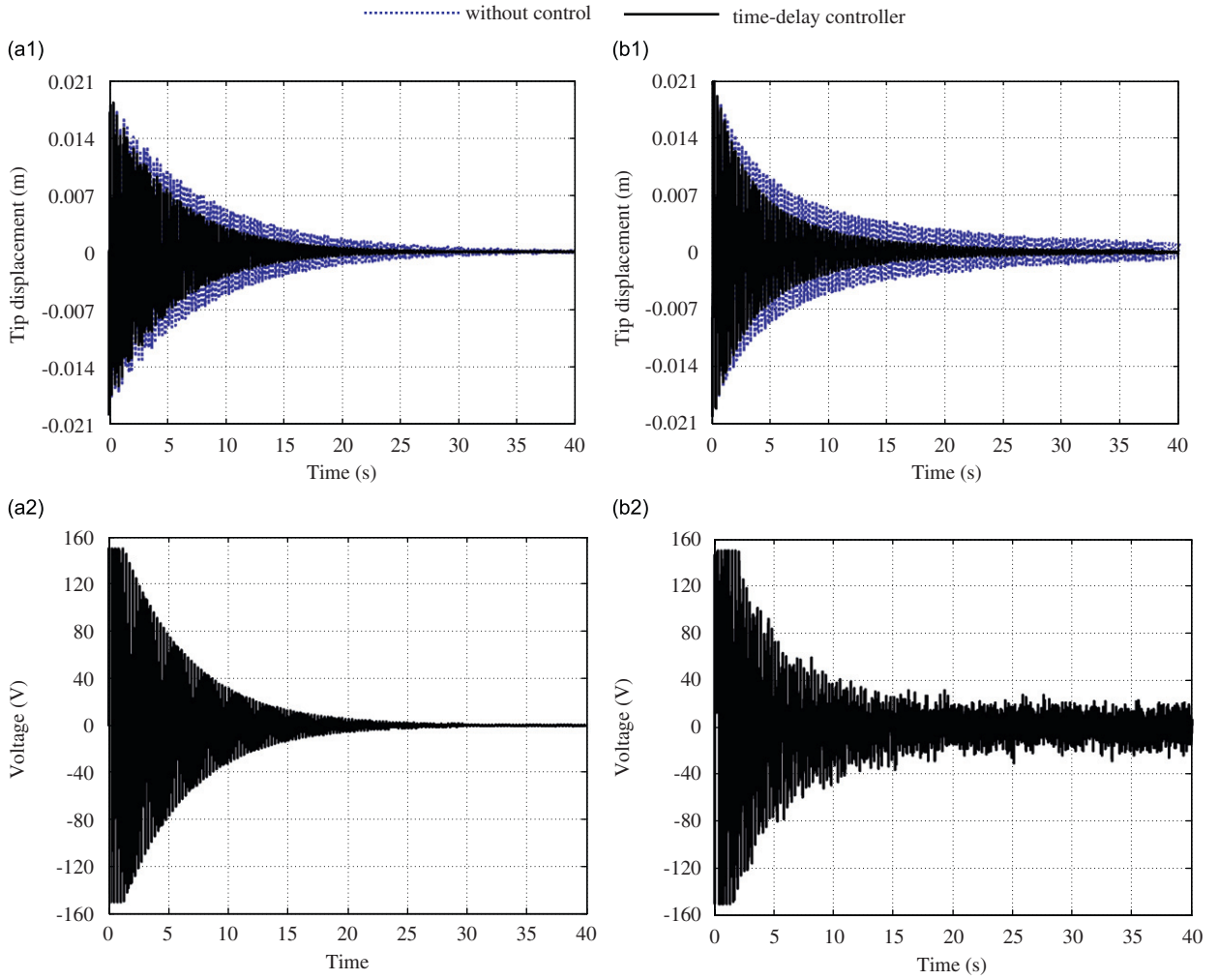

Fig. 6. Response of the plate and applied voltage of Actuator I using the time-delay controller to control the plate with time delay ($\lambda_1 = 0.005$ s, one actuator case): (a) simulation result and (b) experimental result.

For this case, Eq. (36) becomes

$$w(x,y,t) = \frac{2}{h}[W_1(x,y) \;\; W_2(x,y)] \begin{bmatrix} \dfrac{\partial^2 W_1(x_1,y_1)}{\partial x^2} & \dfrac{\partial^2 W_2(x_1,y_1)}{\partial x^2} \\ \dfrac{\partial^2 W_1(x_2,y_2)}{\partial x^2} & \dfrac{\partial^2 W_2(x_2,y_2)}{\partial x^2} \end{bmatrix}^{-1} \begin{bmatrix} \varepsilon_{x_1} \\ \varepsilon_{x_2} \end{bmatrix} \tag{40}$$

In the experimental and numerical studies, the weighting matrices in Eq. (23) are chosen as $\overline{\mathbf{Q}}_1 = [100, 100, 1, 1]$ and $\overline{\mathbf{Q}}_2 = [3 \times 10^{-6}, 4 \times 10^{-7}]$. The following five cases are considered:

(1b) no time delay in the system; the no-delay controller is used to control the non-time-delay system;

(2b) $\lambda_1 = 0.004$ s and $\lambda_2 = 0.004$ s exist in the system for experimental study and $\lambda_1 = 0.08$ s and $\lambda_2 = 0.08$ s for numerical study; the no-delay controller is used to control the time-delay system;

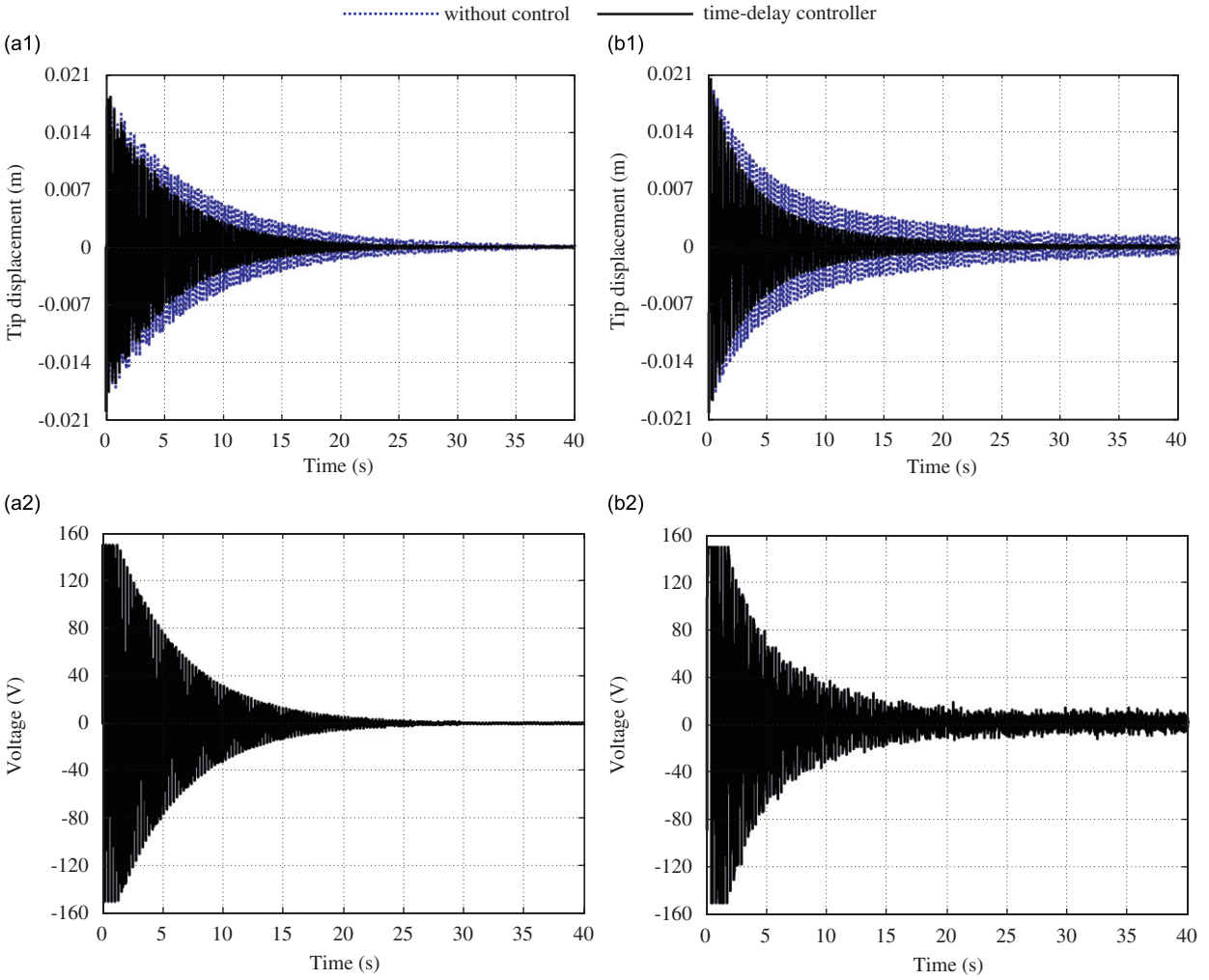

Fig. 7. Response of the plate and applied voltage of Actuator I using the time-delay controller to control the plate with time delay ($\lambda_1 = 0.05$ s, one actuator case): (a) simulation result and (b) experimental result.

(3b) $\lambda_1 = 0.003$ s and $\lambda_2 = 0.008$ s exist for both experimental study and numerical simulation; the time-delay controller is used to control the time-delay system;

(4b) $\lambda_1 = 0.04$ s and $\lambda_2 = 0.02$ s exist for both experimental study and numerical simulation; the time-delay controller is used to control the time-delay system and

(5b) $\lambda_1 = 0.2$ s and $\lambda_2 = 0.4$ s exist for both experimental study and numerical simulation; the time-delay controller is used to control the time-delay system.

In the experiments, data sampling period is set to be $T = 0.001$ s for the cases (1b)–(4b) and $T = 0.005$ s for the case (5b).

The responses of the down-right point of the plate and the applied voltages of the two actuators are demonstrated in Figs. 9–13. The same conclusions as those in Figs. 4–8 may be also obtained in Figs. 9–13.

There are few more questions that need to be mentioned and discussed herein: (1) The time delay used in the experimental studies of this paper is voluntarily introduced in the control system and is not the inherent delay

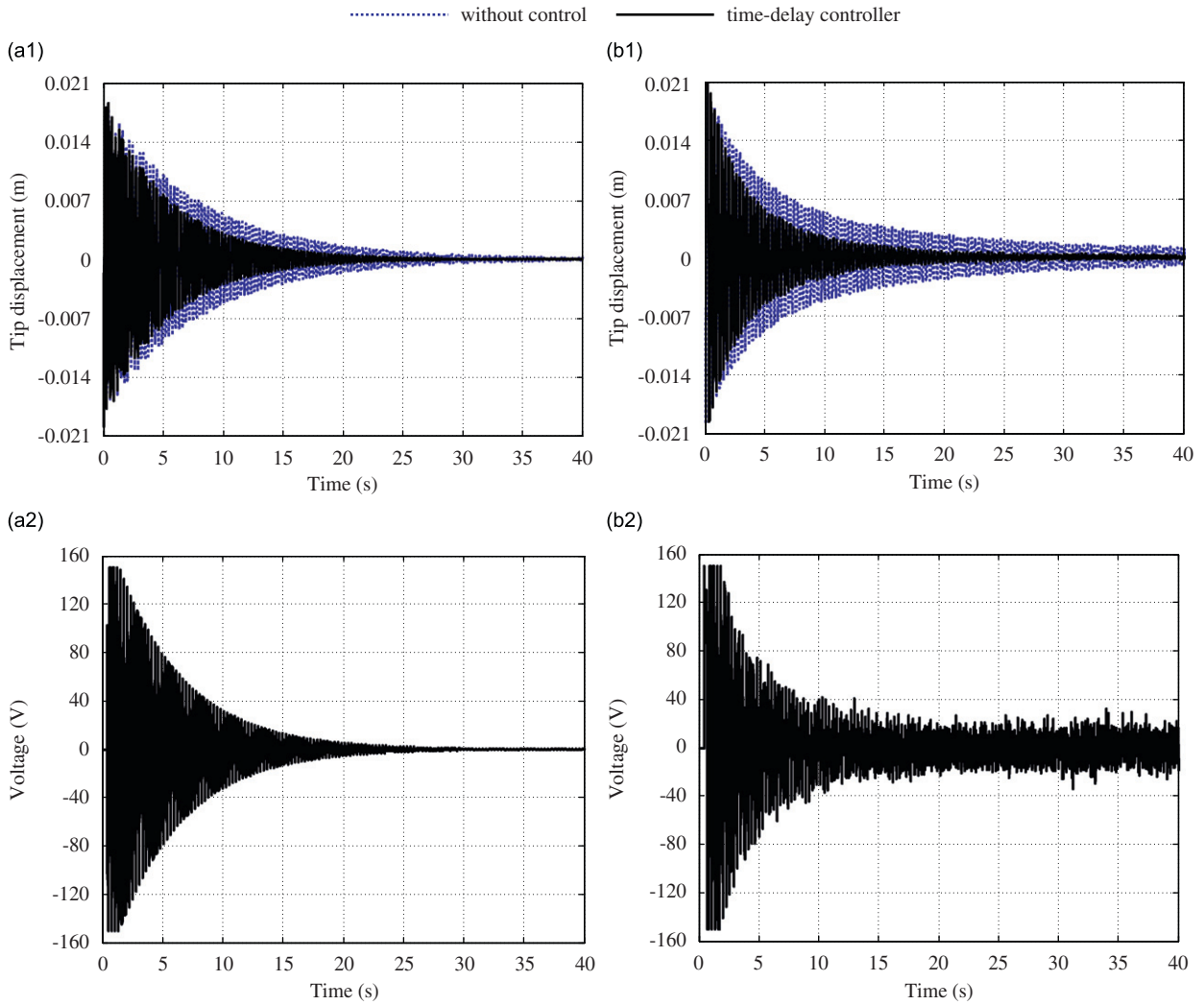

Fig. 8. Response of the plate and applied voltage of Actuator I using the time-delay controller to control the plate with time delay ($\lambda_1 = 0.4$ s, one actuator case): (a) simulation result and (b) experimental result.

within. There should exist an inherent delay in the experiment system which is believed to be minimum and was not taken into account in this paper. (2) The determination of inherent delay in control systems is actually so-called time-delay identification problem which is not only a critical but a challenging topic for delayed system dynamics. Up to now, the study on this topic is very limited, only few theoretical studies have been done [24,25] and there is no experiment study yet. Furthermore, the inherent delay in a control system is possibly time-varying. When doing experiment on it, one may also encounter some uncertain factors such as model error and signal noise, etc. So it would be very hard to exactly determine the inherent delay of the system by experiments. (3) The time-delay controller proposed in this paper should be re-designed for every different delay. In addition, this controller cannot deal with time-varying delay since it is designed based on the LQR method. (4) In practice, time delay in control systems is usually little and is possibly varying within some extent. Therefore, a time-delay controller using a control strategy with strong robustness to structural parameter and external disturbance might have some robustness to the variance of time delay. This remains to be further worked on.

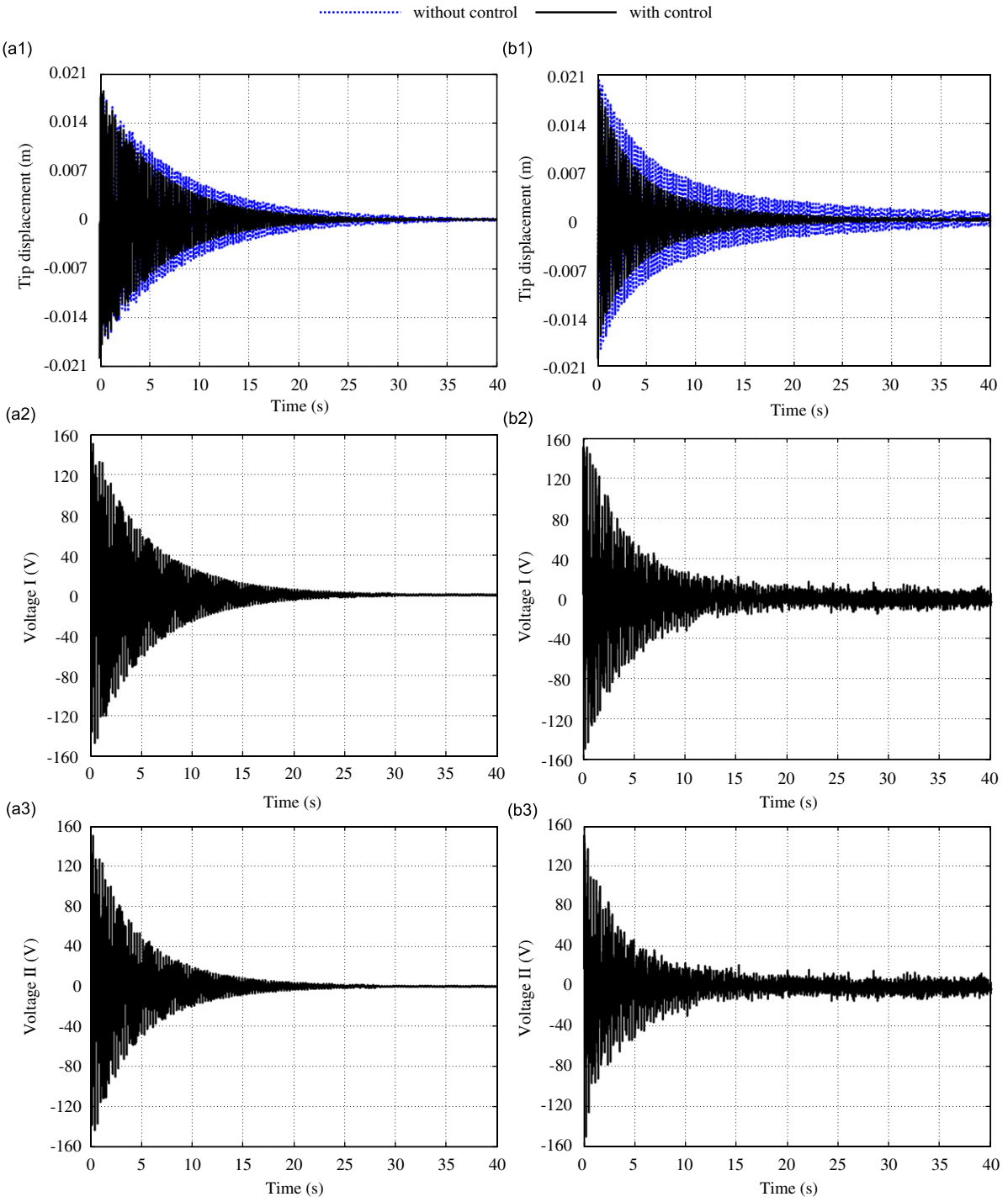

Fig. 9. Response of the plate and applied voltages of the two actuators using the no-delay controller to control the plate without time delay (two actuators case): (a) simulation result and (b) experimental result.

6. Concluding remarks

In this paper, delayed feedback control is numerically and experimentally studied using a flexible plate as research object. Optimal positions of actuators are determined using the PSO. A controller with multiple time

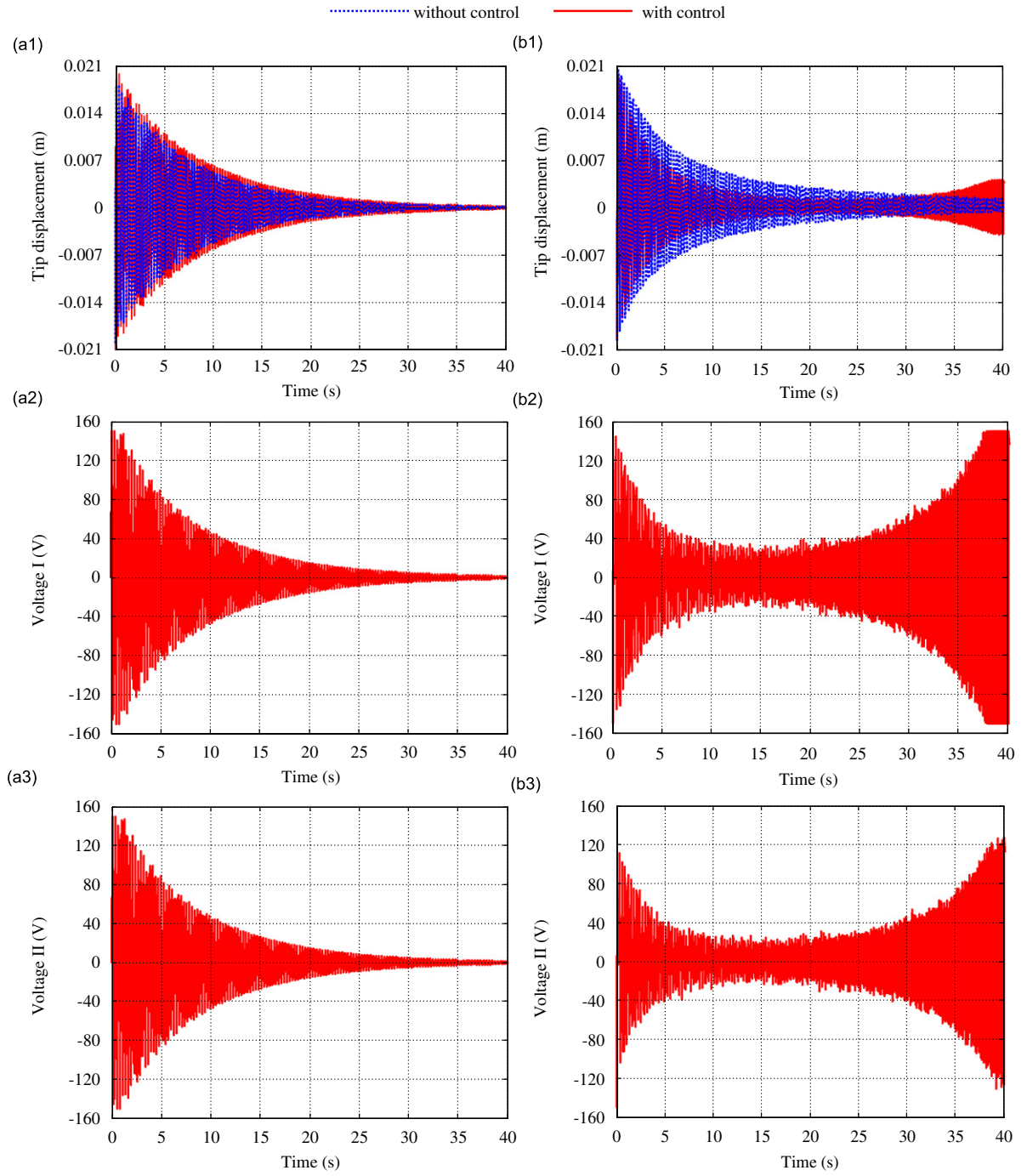

Fig. 10. Response of the plate and applied voltages of the two actuators using the no-delay controller to control the plate with time delays (two actuators case): (a) simulation result ($\lambda_1 = 0.08$ s and $\lambda_2 = 0.08$ s) and (b) experimental result ($\lambda_1 = 0.004$ s and $\lambda_2 = 0.004$ s).

delays is presented. An experiment system based on a DSP board is introduced. Numerical and experimental results show that time delay in control systems may cause the degradation of control efficiency if it is not treated in control design. Delayed feedback control is a feasible strategy that may be used for structural control.

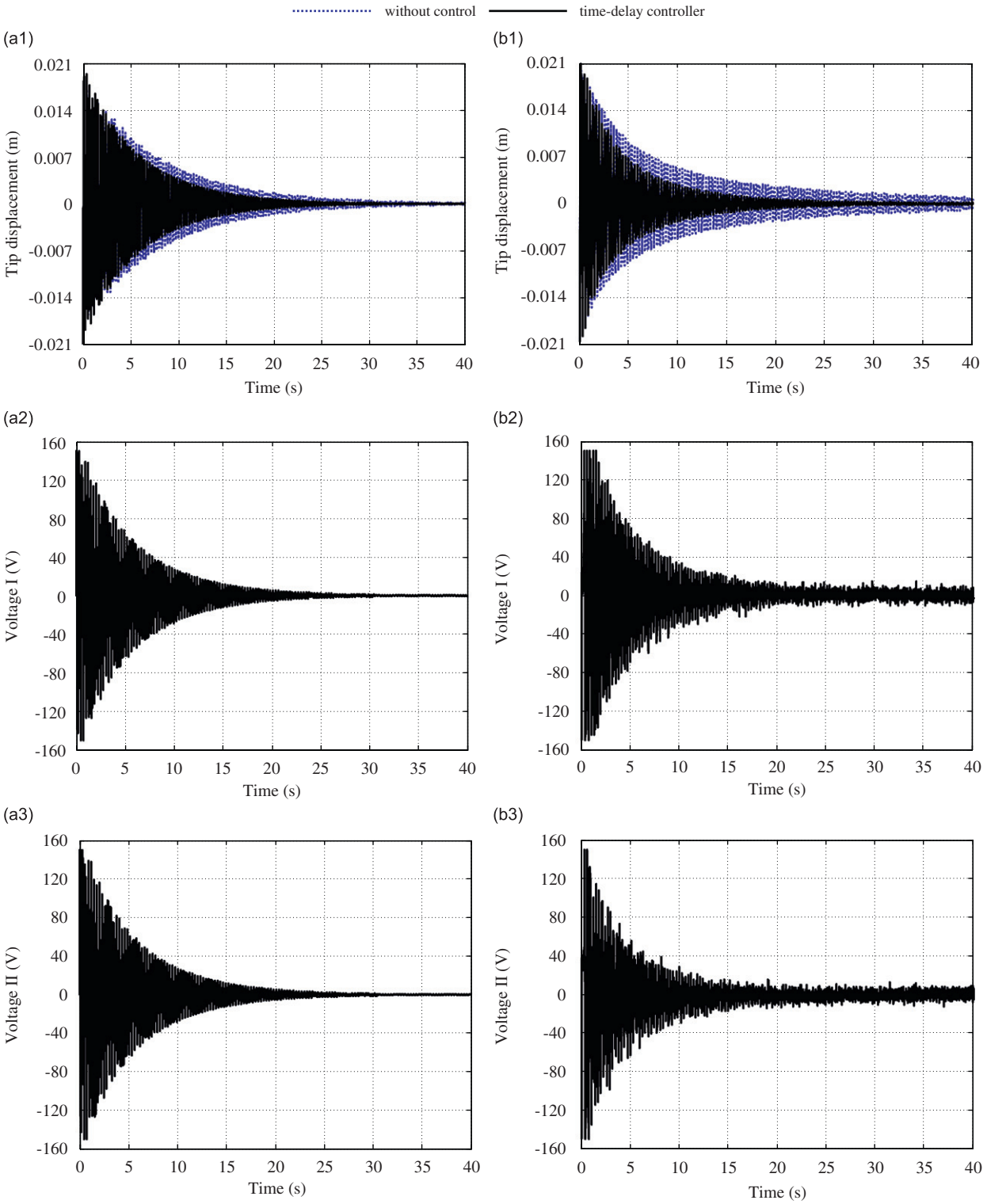

Fig. 11. Response of the plate and applied voltages of the two actuators using the time-delay controller to control the plate with time delays ($\lambda_1 = 0.003$ s and $\lambda_2 = 0.008$ s, two actuators case): (a) simulation result and (b) experimental result.

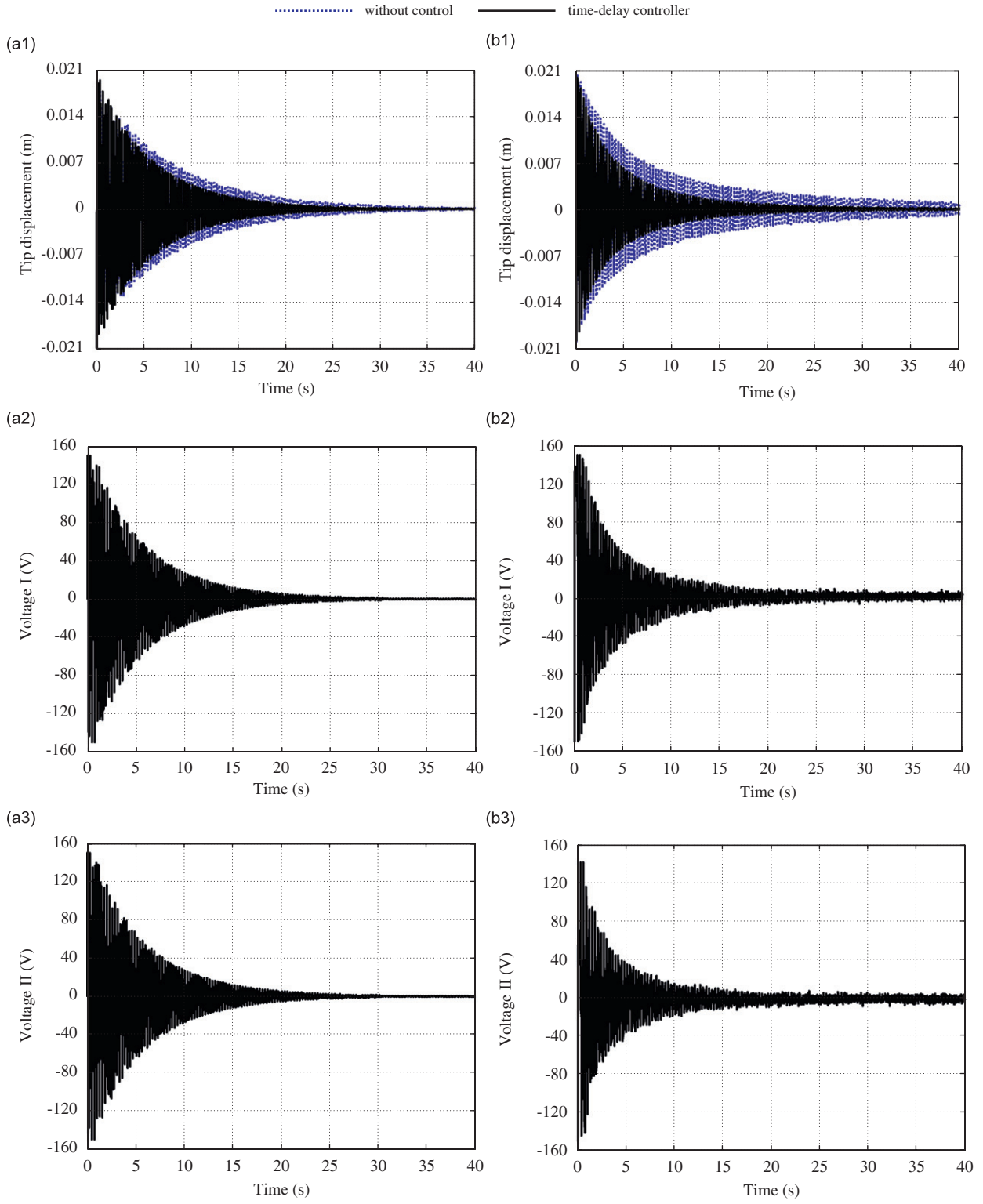

Fig. 12. Response of the plate and applied voltages of the two actuators using the time-delay controller to control the plate with time delays ($\lambda_1 = 0.04$ s and $\lambda_2 = 0.02$ s, two actuators case): (a) simulation result and (b) experimental result.

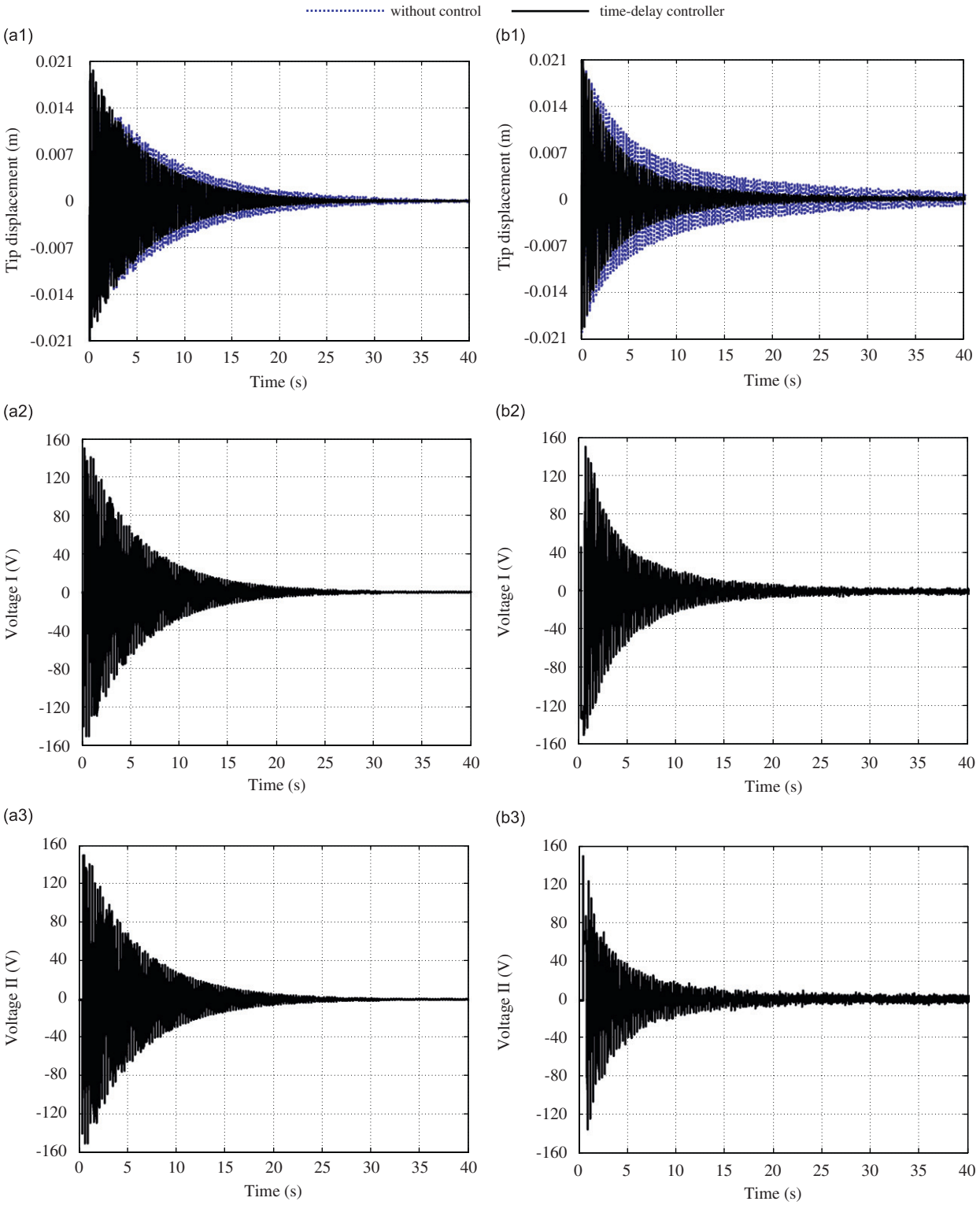

Fig. 13. Response of the plate and applied voltages of the two actuators using the time-delay controller to control the plate with time delays ($\lambda_1 = 0.2$ s and $\lambda_2 = 0.4$ s, two actuators case): (a) simulation result and (b) experimental result.

Acknowledgments

The work described in this paper was supported by a grant from Science Foundation of China (10772112, 10472065), the Key Project of Ministry of Education of China (107043), the Key Scientific Project of Shanghai Municipal Education Commission (09ZZ17) and the Specialized Research Fund for the Doctoral Program of Higher Education of China (20070248032).

References

[1] H.Y. Hu, Z.H. Wang, *Dynamics of Controlled Mechanical Systems with Delayed Feedback*, Springer, Berlin, 2002.
[2] M. Abdel-Rohman, Time-delay effects on active damped structures, *Journal of Engineering Mechanics* 113 (11) (1987) 1709–1719.
[3] L.L. Chung, A.M. Reinhorn, T.T. Soong, Experiments on active control of seismic structures, *Journal of Engineering Mechanics, ASCE* 114 (2) (1988) 241–256.
[4] S. Mc Greery, T.T. Soong, A.M. Reinhorn, An experiments study of time delay compensation in active structural control, *Proceedings of the Sixth International Modal Analysis Conference*, *SEM*, 1988, pp. 1733–1739.
[5] G.P. Cai, J.Z. Huang, Optimal control method for seismically excited building structures with time-delay in control, *Journal of Engineering Mechanics, ASCE* 128 (6) (2002) 602–612.
[6] G.P. Cai, J.Z. Huang, S.X. Yang, An optimal control method for linear systems with time delay, *Journal of Computers and Structures* 81 (15) (2003) 1539–1546.
[7] Z.M. Ge, C.L. Hsiao, Y.S. Chen, Nonlinear dynamics and chaos control for a time delay Duffing system, *International Journal of Nonlinear Sciences and Numerical Simulations* 6 (2) (2005) 187–199.
[8] M. Xiao, J.D. Cao, Bifurcation analysis and chaos control for Lu system with delayed feedback, *International Journal of Bifurcation and Chaos* 17 (12) (2007) 4309–4322.
[9] J. Xu, K.W. Chung, Effects of time delayed position feedback on a van der Pol–Duffing oscillator, *Physica D* 18 (1–2) (2003) 17–39.
[10] M. Hosek, N. Olgac, A single-step automatic tuning algorithm for the delayed resonator vibration absorber, *IEEE/ASME Transactions on Mechatronics* 7 (2) (2002) 245–255.
[11] Y.Y. Zhao, J. Xu, Effects of delayed feedback control on nonlinear vibration absorber system, *Journal of Sound and Vibration* 308 (2007) 212–230.
[12] G.P. Cai, C.W. Lim, Optimal tracking control of flexible hub–beam system with time delay, *Multibody System Dynamics* 16 (4) (2006) 331–350.
[13] F. Yuan, Effects of Delayed Feedback Control on Stability in the Cantilever Pipe Conveying Fluid, Master Thesis, Tongji University, 2008 (in Chinese).
[14] Z.H. Wang, H.Y. Hu, Stabilization of vibration systems via delayed state difference feedback, *Journal of Sound and Vibration* 296 (1–2) (2006) 117–129.
[15] J. Xu, K.W. Chung, C.L. Chan, An efficient method for studying weak resonant double Hopf bifurcation in nonlinear systems with delayed feedbacks, *SIAM Journal of Applied Dynamical Systems* 6 (1) (2007) 29–60.
[16] Z.C. Qiu, X.M. Zhang, H.X. Wu, H.H. Zhang, Optimal placement and active vibration control for piezoelectric smart flexible cantilever plate, *Journal of Sound and Vibration* 301 (2007) 521–543.
[17] S. Leleu, H. Abou-Kandil, Y. Bonnassieux, Piezoelectric actuators and sensors location for active control of flexible structures, *IEEE Transaction on Instrument and Measurement* 50 (6) (2001) 1577–1582.
[18] Y. Wang, Z.M. Dong, H.Z. Li, D.M. Sun, Optimum disposition of sensor/actuator for active vibration control of flexible structure, *Journal of Nanjing University of Science and Technology* 26 (2002) 29–35 (in Chinese).
[19] J. Kennedy, R. Eberhart, Particle swarm optimization, *IEEE International Conference on Neural Networks*, 1995, pp. 1942–1948.
[20] M.A. Abido, Optimal design of power-system stabilizers using particle swarm optimization, *IEEE Transactions on Energy Conversion* 17 (3) (2002) 406–413.
[21] Y. Shi, R. Eberhart, A modified particle swarm optimizer, *IEEE World Congress on Computational Intelligence*, 1998, pp. 69–73.
[22] Z.Q. Sun, *Theory and Application of Computer Control*, Tsinghua University Press, Beijing, 1989 (in Chinese).
[23] J.Q. Han, L.L. Yuan, The discrete form of tracking-differentiator, *Journal of Systems Science and Mathematical Sciences* 19 (3) (1999) 268–273 (in Chinese).
[24] S.V. Drakunov, W. Perruquetti, J.P. Richard, L. Belkoura, Delay identification in time-delay systems using variable structure observers, *Annual Reviews in Control* 30 (2006) 143–158.
[25] H.Y. Hu, Identifiability of feedback delays of linear controlled systems, *Chinese Journal of Vibration Engineering* 14 (2) (2001) 161–165 (in Chinese).